DEVELOPMENT OF A MULTI-BODY STATISTICAL SHAPE MODEL OF THE WRIST

Anton Semechko[1,2], Anne Agur[2], Robert Dony[1], Michele Oliver[1]

[1] School of Engineering, University of Guelph, Guelph, Ontario N1G 2W1, Canada
[2] Division of Anatomy, Faculty of Medicine, University of Toronto, Toronto, Ontario M5S 1A8, Canada

1. INTRODUCTION

In the last decade, increased availability of high performance computing resources has prompted a shift in the experimental approach across multiple scientific disciplines to the point where computer-based simulations are gradually becoming acceptable substitutes to traditional lab bench experiments. The field of computational biomechanics is one derivative of this technological evolution and has been successfully applied to biomedical problems such as impact and fracture mechanics of bone, load transmission through the joints, feasibility of joint replacements, investigation of joint injury mechanisms, and many others. Despite remarkable advances in this domain, there remain a number of challenges. One of those is related to the fact that almost all biomechanical models reported in literature to date were derived from the anatomy of a single individual. This is a conceptually problematic issue because the results acquired from the simulations based on subject-specific models cannot be generalized to a wider population set. Statistical shape modeling (SSM) is a well established image segmentation technique and provides an intuitive approach for creating population-based parametric models [1]. Within this framework the notion of "mean shape" and "principal components of shape" are explicitly defined and can be used as population representatives for finite element (FE) simulations.

The main objective of the current study was concerned with the development of a parametric, anatomically accurate, FE model of the human hand and wrist. As a first step in this direction, we used a publically available database of wrist bone anatomy [2] to construct a multi-body SSM of the human wrist. The resulting model provides an efficient parameterization of anatomical variations of the entire training set and can thus overcome major shortcoming of conventional biomechanical models associated with limited generalization ability. The main contributions of this work are:

- **A novel algorithm for resampling closed genus-0 meshes to produce high quality triangulations of arbitrary complexity suitable for FE simulations**.

- **A robust method for constructing multi-body SSM of the wrist from surface meshes**.

Additionally, all procedures developed in the course of this study could be directly applied to create an equivalent, multi-body statistical model of the ankle.

2. MATERIALS AND METHODS

The data used in this study came in the form of triangular surface meshes extracted from CT scans of 30 healthy volunteers [2]. Unfortunately, most of these meshes had large numbers of nearly degenerate triangles (i.e. triangles whose vertices are almost collinear) which corrupted the quality and increased mesh complexity by a considerable amount (in fact such elements are abundant in meshes extracted directly from segmented medical images using conventional methods like marching cubes algorithm [3]). If left unchecked, these artifacts would have an adverse effect on the computational efficiency of all subsequent operations. Furthermore, the models built in this study were ultimately intended for use with finite element methods (FEM). The numerical stability and convergence of FEM, however, largely depend on the quality of the input meshes [4]. For this reason, we needed a robust mesh resampling algorithm that would address the issues of quality and complexity simultaneously. The lack of easily implementable algorithms that could concurrently address these concerns, inspired us to develop our own remeshing technique. The steps involved in this procedure are summarized in subsection 2.1.

Upon completing initial preprocessing of the input meshes we could proceed to construct the composite SSM of the wrist. This task was complicated by the fact that carpal (i.e. wrist) bones have non-negligible relative motion as the wrist changes from one posture to the next. Additionally, although the wrists from different individuals may appear to be in the same posture, in general, the spatial relationships between the bones in these wrists will not be the same [2].

Recognition of this fact is important because the SSMs must be constructed using the training shapes which are normalized with respect to the similarity transformations. If this requirement is not satisfied the statistical model will not provide a valid description of the true anatomical variations encountered in the training set. Due to the complexity of this problem, we decomposed it into two parts. The first of these is summarized in subsection 2.2 and deals with the construction of SSMs of the individual wrist bones. The second part is described in subsection 2.3 and addresses the core problem of appropriately merging individual carpal bones into a composite SSM of the entire wrist.

2.1 Mesh Resampling

The proposed resampling procedure is realized by combining the properties of conformal maps from differential geometry with the physical principles governing the dynamics of charged particle systems.
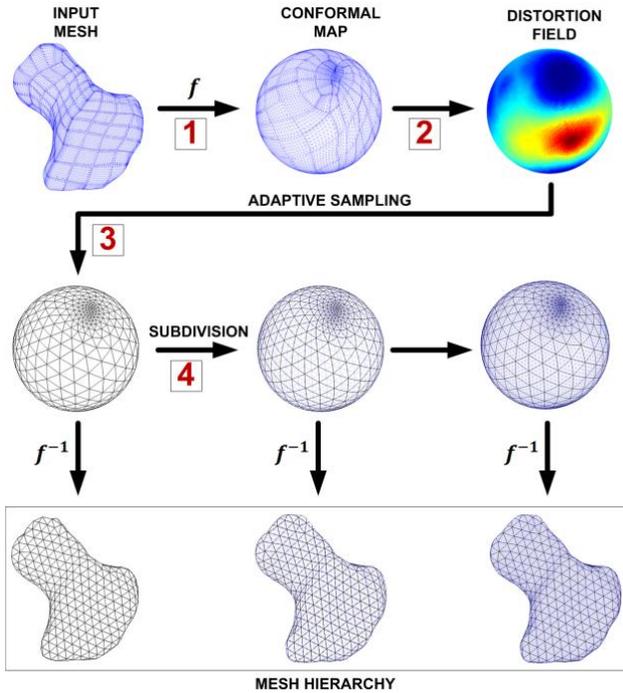
Figure 1: Four main stages of the resampling procedure: (1) conformal parameterization, (2) calculation of the distortion field at the vertices of the input mesh, (3) adaptive sampling of the parameter domain using a system of charged particles, (4) subdivision and regularization (optional).

As illustrated in Figure 1, the algorithm consists of four consecutive stages that include:

(1) *Calculation of a conformal map (CM) of the input mesh* (see [5] for more details).

(2) *Calculation of the distortion field (DF) induced by CM from step 1*. DF is a scalar "charge" field defined on S^2 and is computed as a product of local length and area distortions.

(3) *Adaptive sampling of the parameter domain using DF from step 2*. This procedure is based on gradient descent minimization of a slightly generalized version of the electrostatic potential energy functional,

$$U_s = \sum_{i}^{N} \sum_{j \neq i}^{N} \frac{q_i q_j}{d_{ij}^s} \qquad (1)$$

where $q_i, q_j : S^2 \to \mathbb{R}^+$ are the position dependent "charges" between the i-th and j-th particles, d_{ij} is the geodesic distance between the particles and $s > 0$ is a (global) parameter used to control the strength of particle interactions.

(4) *Subdivision and regularization*. Once the particles have been fixed on the unit sphere, their positions determine the vertices of the base mesh in the parameter domain. Surfaces of increasing complexity can be recovered by iteratively subdividing this mesh with any standard subdivision scheme and then mapping the result back to original surface. Finally, regularization is performed only if two or more subdivisions are required and is achieved by relaxing the subdivided mesh (in the parameter domain) with a few gradient descent iterations of Tutte energy [5].

2.2 Statistical Models of Individual Carpal Bones

One of the simplest and perhaps most popular ways of representing a shape, $S_i \subset \mathbb{R}^3$, is by a set of points sampled from its surface, $V_i = \{ \boldsymbol{v}_j \in S_i \mid j = 1, \dots, N \}$. In the context of statistical shape modeling, this type of representation is commonly termed the point distribution model (PDM). Given a set a training set of sample PDMs, $T = \{ V_i \mid i = 1, \dots, M \}$, the space of geometric variations of an object can be learned using principal component analysis. For example, suppose $\boldsymbol{V}_i$ is a shape vector composed of an ordered list of corresponding PDM vertices (normalized with respect to the similarity transformation group) such that $\boldsymbol{V}_i = [\boldsymbol{v}_{i1}, \dots, \boldsymbol{v}_{iN}]^T$ where $\boldsymbol{v}_{ij} = (x_{ij}, y_{ij}, z_{ij})$ and N is the total number of vertices. Then the shape covariance matrix can be defined as follows:

$$\boldsymbol{C} = \frac{1}{M-1} \sum_{i=1}^{M} (\boldsymbol{V}_i - \overline{\boldsymbol{V}})(\boldsymbol{V}_i - \overline{\boldsymbol{V}})^T \qquad (2)$$

$$\overline{\boldsymbol{V}} = \frac{1}{M} \sum_{i=1}^{M} \boldsymbol{V}_i \qquad (3)$$

A linear SSM is simply a weighted sum of the mean shape vector ($\overline{V}$) and the first k most important eigenvectors (a.k.a. eigenmodes) of C,

$$V = \overline{V} + \sum_{i=1}^{k} b_i p_i \quad , 1 \leq k \leq M - 1 \qquad (4)$$

where $\{p_i\}$ are the eigenvectors of C, and $\{b_i\}$ are the shape parameters used to control the geometry of the object by modifying the contribution of the individual eigenmodes.

In order to derive meaningful and accurate information regarding the shape variability, the points $\{v_{ij}\} \forall \ i \in [1, M]$ must be situated in semantically equivalent anatomical positions. Establishing such a correspondence is in fact the most challenging aspects of the entire model building process. In this study, dense point correspondence was established using a procedure composed of the following steps:

(1) Rigid pairwise registration using distance fields.

(2) Normalization of conformal parameterizations with respect to the Möbius transformation group.

(3) Groupwise point correspondence optimization.

The first step pre-aligned the surfaces using similarity transformations and was designed with the considerations of robustness and reusability. Although the utility of the first criterion is self-explanatory, the reusability feature is meant to allow parts of the procedure to be integrated into the later model building stages (see subsection 2.3). The second step is meant to ensure that parameterizations of the training shapes are also pre-aligned thus providing good initialization to the groupwise optimization procedure that followed. The last step was the most computationally intensive of all and ultimately determined the final quality of the SSMs. It was based on the idea that shape parameterizations can be modified independently of the primary shapes and was largely based on the minimum description length optimization method described in [6].

2.3 Composite Statistical Model of the Wrist

In a healthy wrist, a pair of articulating bones usually have congruent articulating surfaces, implying that the local geometries of adjacent bones are highly correlated. In view of the fact that there are eleven tightly coupled inter-carpal articulations, altering the geometry of a single carpal bone is likely to produce a cascading effect through the entire wrist, implying additional correlations between non-neighbouring bones. In order to accurately capture these relationships, prior to construction of the composite

SSM, the individual bones in all sample wrists must be aligned to the same pose while retaining valid physiological inter-relationships. To meet this requirement, we built around the idea that during motion, articulating surfaces between two adjacent bones must remain coincident [7] and developed a new, constrained, groupwise, two-step registration scheme. First, we used the correspondences established between the individual carpal bones to perform unconstrained, *sequential,* groupwise registration of all sample wrists. Subsequently, we used the distance fields computed during the earlier stage (see subsection 2.2) to estimate articulating surfaces and then used these surfaces to impose the physiological constraints while searching for the solution closest to the one obtained during the first (unconstrained registration) step.

3. RESULTS & DISCUSSION

3.1 Mesh Resampling

In this study, we used our new remeshing algorithm to resample 239 meshes of the carpal bones of the right hand. As an example, Figure 2 shows side by side comparisons of three different carpal bones before and after resampling. Table 1 provides a corresponding summary of the changes in mesh complexity, quality and approximation errors as measured by the difference in surface area and volume. To assess the quality of the meshes, we used the minimum triangle aspect ratios (η) [4]. According to this measure equilateral triangles are the most desirable and have $\eta = 1$.

$$\eta = 2 \frac{inscribed \ radius}{circumscribed \ radius} \qquad (5)$$

The results summarized in Table 1 are entirely representative of the remaining 236 carpal bones used in this study and show a dramatic improvement in mesh quality at the cost of minor errors (less than 0.30%) in volume and surface area.

3.2 Composite Statistical Model of the Wrist

The visualization of the multi-body SSM of the wrist is provided in Figure 3. Based on the observed pattern of variations, it can be seen that the most pronounced changes occur as a result of 'widening' and 'narrowing' of the carpal bone complex in the lateral directions. Another interesting observation is that that approximately 74% of the structural variations of the carpus could be described by only four eigenmodes. We believe that this would not have been possible without the local and non-local geometric correlations that exist between the carpal bones.
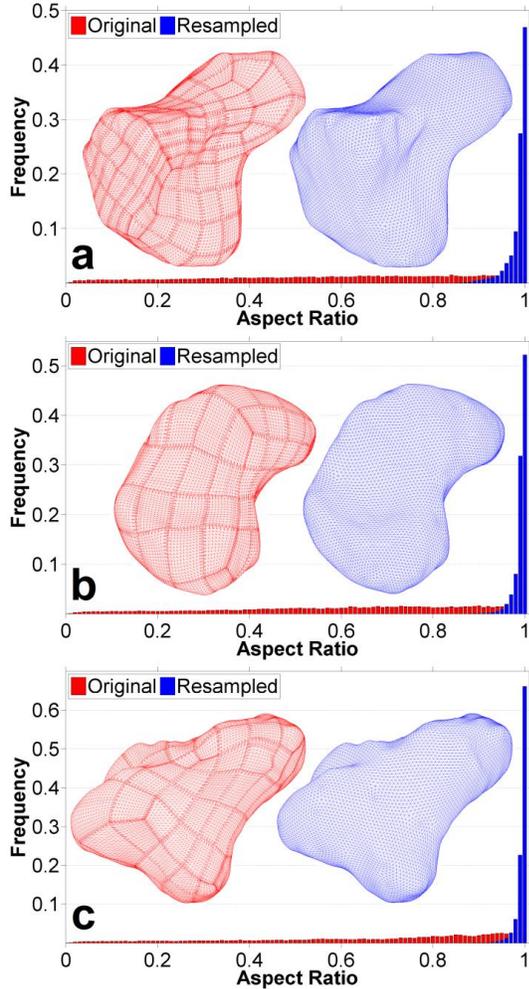
Figure 2: Original and resampled surface meshes with corresponding triangle aspect ratio distributions; (a) *hamate*, (b) *scaphoid*, (c) *trapezium*. Base meshes of the resampled objects shown in (a-c) contained 500 vertices. In all instances, the final mesh was obtained by subdividing the base mesh two times.

Table 1: Mesh complexity, quality and reconstruction errors before and after resampling of objects shown in Figure 2. 'O' stands for original and 'R' for resampled. η_{min} = minimum triangle aspect ratio. AE = surface area error = $(A_R/A_O - 1)*100$. VE = volume error = $(V_R/V_O - 1)*100$.

Obj		# verts	# faces	η_{min}	AE (%)	VE (%)
a	O	39548	19776	0.001	-0.276	-0.116
	R	**15936**	**7970**	**0.797**		
c	O	31068	15936	0.005	-0.190	-0.102
	R	**15936**	**7970**	**0.883**		
d	O	32820	16412	0.001	-0.200	-0.100
	R	**15936**	**7970**	**0.886**		

4. CONCLUSION & FUTURE WORK

This study was a stepping stone toward the ultimate goal of creating an anatomically accurate, parametric FE model of the hand and wrist. To this end, we proposed a novel mesh resampling procedure and also developed a new technique for coupling multiple, statistical carpal bone models within a single, physiologically valid model of the entire wrist. While the performance of our algorithms was demonstrated on a publically available database of the wrist bones [2], they are directly generalizable to the multi-body skeletal structures of the lower limb. In the future, we intend to build upon these methods to construct a statistical, FE model of the upper limb (hand, wrist and forearm) that in addition to the bony structures will incorporate the connective and muscle tissues.

REFERENCES

[1] Davies, R.H., Twining, C.J., Taylor, C.J. (2008) *Statistical Models of Shape - Optimization and Evaluation*, 1st ed., London: Springer-Verlag.
[2] Moore, D.C., Crisco, J.J., Trafton, T.G., Leventhal, E.L. (2007) "A digital database of wrist bone anatomy and carpal kinematics", *Journal of Biomechanics*, Vol. 40, pp. 2537-2542.
[3] Meyer, M., Kirby, R.M., Whitaker, R. (2007) "Topology, accuracy, and quality of isosurface meshes using dynamic particles", *IEEE Transactions on Visualization and Computer Graphics*, Vol. 13, pp. 1704 - 1711.
[4] Shewchuk J.R. "What is a good linear element? Interpolation, conditioning, and quality measures", in: 11th International Meshing Roundtable, pp. 115-126. Sandia National Laboratories, Ithaca, New York (2002)
[5] Gu, X., Wang, Y., Chan, T.F., Thompson, P.M., Yau, S.-T. (2004) "Genus zero surface conformal mapping and its application to brain surface mapping", *IEEE Transactions on Medical Imaging*, Vol. 23, pp. 949-958.
[6] Heimann, T., Wolf, I., Williams, T.G., Meinzer, H.P. (2005) '3D active shape models using gradient descent optimization of description length' in *Proceedings of Information Processing in Medical Imaging*, LNCS, Vol. 3565, pp. 566-577: Springer.
[7] Van de Giessen, M., Streekstra, G.J., Strackee, S.D., Maas, M., Grimbergen, K.A., van Vliet, L.J., Vos, F.M. (2009) 'Constrained registration of the wrist joint', *IEEE Transactions on Medical Imaging*, Vol. 28, pp. 1861-1869.
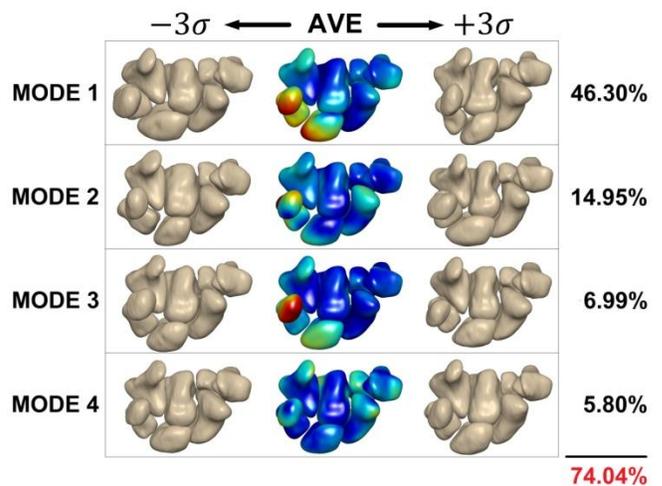
Figure 3: Extremes of the first four principal modes of carpus variation. The structural changes associated with each mode are represented by colourmaps (superimposed on the average carpus) along the middle column. Areas in dark red denote the most amount of variation and areas in dark blue the least amount of variation.